Nanoscale Res Lett (2009) 4:550–557
DOI 10.1007/s11671-009-9279-9

NANO EXPRESS

Self-Assembled 3D Flower-Like Hierarchical β-Ni(OH)$_2$ Hollow Architectures and their In Situ Thermal Conversion to NiO

Lu-Ping Zhu · Gui-Hong Liao · Yang Yang · Hong-Mei Xiao · Ji-Fen Wang · Shao-Yun Fu

Received: 16 January 2009 / Accepted: 11 February 2009 / Published online: 27 February 2009

Abstract Three-dimensional (3D) flower-like hierarchical β-Ni(OH)$_2$ hollow architectures were synthesized by a facile hydrothermal route. The as-obtained products were well characterized by XRD, SEM, TEM (HRTEM), SAED, and DSC-TGA. It was shown that the 3D flower-like hierarchical β-Ni(OH)$_2$ hollow architectures with a diameter of several micrometers are assembled from nanosheets with a thickness of 10–20 nm and a width of 0.5–2.5 μm. A rational mechanism of formation was proposed on the basis of a range of contrasting experiments. 3D flower-like hierarchical NiO hollow architectures with porous structure were obtained after thermal decomposition at appropriate temperatures. UV–Vis spectra reveal that the band gap of the as-synthesized NiO samples was about 3.57 eV, exhibiting obviously red shift compared with the bulk counterpart.

Keywords Ni(OH)$_2$ · NiO · Hollow architecture · Hydrothermal synthesis

L.-P. Zhu (✉) · J.-F. Wang
School of Urban Development and Environmental Engineering, Shanghai Second Polytechnic University, Shanghai 201209, China
e-mail: lpzhu@eed.sspu.cn; lpzhu@mail.ipc.ac.cn

L.-P. Zhu · G.-H. Liao · Y. Yang · H.-M. Xiao · S.-Y. Fu
Technical Institute of Physics and Chemistry, Chinese Academy of Sciences, Beijing 100190, China

S.-Y. Fu
e-mail: syfu@mail.ipc.ac.cn

Introduction

Ordered self-assembly of nanoscale building blocks, such as nanoparticles, nanorods, nanoribbons, and so forth, into complex architectures has recently become a hot topic in material research fields. Remarkable progress has been made in the self-assembly of highly organized building blocks of metals [1–4], semiconductors [5–8], copolymers [9], and organic–inorganic hybrid materials [10] based on different driving mechanisms, such as Ostwald ripening [11], Kirkendall effect [12], and self-assembly of nanoscale blocks through hydrophobic interactions [13]. However, controlled organization into curved hollow structures from the primary building units, for example sheets, remains a challenge for materials self-assembly [14]. The ability to assemble primary units into hollow structures is in great demand not only because of their role in better understanding the concept of self-assembly with artificial building blocks but also due to its great potential for technological applications [15].

Nickel hydroxide (Ni(OH)$_2$), as one of the most important transition metal hydroxides, has received increasing attention due to its extensive applications, especially as a positive electrode active material, in alkaline rechargeable Ni-based batteries [16]. It has been reported that the capacity of the positive electrode could be significantly increased when nanophase Ni(OH)$_2$ was added to micrometer-size spherical Ni(OH)$_2$ [17, 18]. Further efforts have focused on searching for new synthetic methods of Ni(OH)$_2$ nanocrystals with high quality and various exciting morphologies. 1D, 2D, and 3D nanostructures of Ni(OH)$_2$, including nanorods [19], nanoribbons [20], nanotubes [21], nanosheets [22], and superstructures patterns [23–28], have been fabricated successfully by a variety of methods. Nickel oxide (NiO) is

a very prosperous inorganic material which was widely applied in the fields of smart window, electrochemical supercapacitor, battery cathodes, catalyst, etc. [29–32]. NiO can be conveniently prepared by thermal decomposition of its precursors [33]. By contrast, there are only limited reports concerning the synthesis of $Ni(OH)_2$ and NiO hollow architectures and their interesting properties. For example, Wang's group synthesized hollow architectures of $Ni(OH)_2$ with unusual form and hierarchical structures by using styrene-acrylic acid copolymer (PSA) latex particles as the templates [23]. Hierarchically porous β-$Ni(OH)_2$ microspheres constructed with nanoflakes were recently prepared with the help of hexamethylenetetramine (HMTA) as the basic source, exhibiting small blue shift compared with the bulk counterpart [24]. Duan et al. reported the fabrication of hierarchical $Ni(OH)_2$ monolayer hollow-sphere arrays with a fine structure of nanoflakelets by an electrochemical strategy based on a polystyrene (PS) sphere colloidal monolayer. Such hierarchically structured hollow-sphere arrays have demonstrated a tunable optical transmission stop band in the visible-near-IR (Vis–NIR) region from 455 to 1855 nm, depending on the hollow-sphere size and the fine structure [25]. However, hollow structures prepared from hard templating routes (e.g. PS latex particles) usually suffer from disadvantages related to high cost and tedious synthetic procedures, which may prevent them from being used in large-scale applications [11]. Thus, it still remains a challenge to develop simple approaches to synthesize hierarchical $Ni(OH)_2$ and NiO hollow architectures.

Herein we describe a facile hydrothermal route to synthesize highly ordered 3D flower-like hierarchical β-$Ni(OH)_2$ hollow architectures with a high yield. The formation mechanism of the 3D flower-like hierarchical β-$Ni(OH)_2$ hollow architectures was proposed. The morphology-retained NiO hollow architectures with porous structure were readily obtained by thermal decomposition of the as-obtained β-$Ni(OH)_2$ products. Finally, the optical property of NiO sample was investigated with the help of UV–Vis spectrum.

Experimental Section

Synthesis of 3D Flower-Like Hierarchical β-$Ni(OH)_2$ and NiO Hollow Architectures

In a typical synthesis, 1 mmol of $NiCl_2{\cdot}6H_2O$ was dissolved in 5 mL of deionized (DI) water, followed by an addition of 15 mL of ethanol and 5 mL of $CO(NH_2)_2$ solution (2 mol L^{-1}) under vigorous stirring. Then, 2 mL of $NH_3{\cdot}H_2O$ (35% by v/v) was added dropwise into the above solution to form a clear blue solution. The final solution was transferred to a 50 mL Teflon-lined autoclave. The autoclave was sealed and heated in an oven at 120 °C for 12 h and then allowed to cool to room temperature. The resulting pale green slurry was rinsed with DI water several times to remove soluble impurities. The product was dried in an oven at 50 °C for 8 h to get the sample of β-$Ni(OH)_2$. To obtain NiO the as-prepared sample of β-$Ni(OH)_2$ was calcined in air for 4 h.

Characterization

The phase purity of the products was examined by X-ray powder diffraction (XRD) using a Rigaku D/max 2500 diffractometer at a voltage of 40 kV and a current of 200 mA with Cu-Kα radiation (λ = 1.5406 Å), employing a scanning rate 0.02°/s in the 2θ ranging from 30 to 80°. Scanning electron microscopy (SEM) images and energy dispersive X-ray (EDX) analysis were obtained using a HITACHI S-4300 microscope (Japan). Transmission electron microscope (TEM) images and the corresponding selected area electron diffraction (SAED) pattern were taken on a Hitachi-600 transmission electron microscope at an accelerating voltage of 200 kV. High-resolution transmission electron microscope (HRTEM) images were carried out for the as-prepared sample using JEOL JEM-2010 transmission electron microscope at an accelerating voltage of 200 kV. The size distribution of the sample was measured using a scale on the magnified SEM micrographs. Thermogravimetric (TGA) and differential scanning calorimetric (DSC) analyses were carried out on a NETZSCH STA-409 PC thermal analyzer with a heating rate of 10 °C min^{-1} in flowing oxygen atmosphere. Room-temperature UV–Vis absorption spectrum was recorded on a Shimadzu UV-1601 PC UV–Vis recording spectrophotometer.

Results and Discussion

The phase structure and purity of the as-synthesized samples were examined by powder XRD. Figure 1 shows the XRD pattern of the samples. It can be seen from Fig. 1 that all of the diffraction peaks can be indexed to a pure hexagonal structure of β-$Ni(OH)_2$ (JCPDS No: 14-0117). No diffraction peaks from impurities are found in the samples.

The morphologies of as-synthesized products were examined by SEM and TEM. Figure 2 shows the SEM images of the β-$Ni(OH)_2$ products. Clearly, the products consist of a high yield of fairly uniform particles with the average size of about 4.5 μm in diameter (Fig. 2a), showing a relatively narrow size distribution (inset of Fig. 2a). The detailed morphologies of the as-synthesized products are shown in Fig. 2b and c, which reveal that all the β-$Ni(OH)_2$ particles have 3D flower-like hierarchical

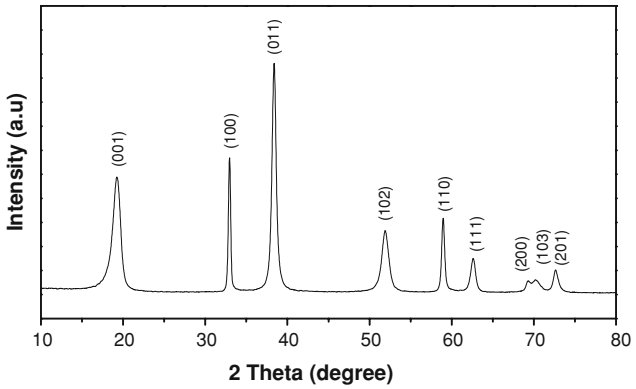

Fig. 1 XRD pattern of the as-obtained β-Ni(OH)$_2$ sample

morphology. Those 3D flower-like architectures are built from several dozen of nanosheets with a thickness of 10–20 nm and a width of 0.5–2.5 μm. The surface of the sheets assembled into the hierarchical micro-architectures was very smooth, probably due to Ostwald ripening [11]. Furthermore, the broken sphere shown in Fig. 2d indicates that the architectures have a hollow structure.

The morphologies and structures of as-synthesized samples were further characterized by TEM. As shown in Fig. 2e, TEM observations demonstrate that the products are flower-like structures similar to the SEM observation. The remarkable feature of the hollow architectures is the obvious contrast between the dark edge and the pale center, as reported for other hollow particles with a central cavity.

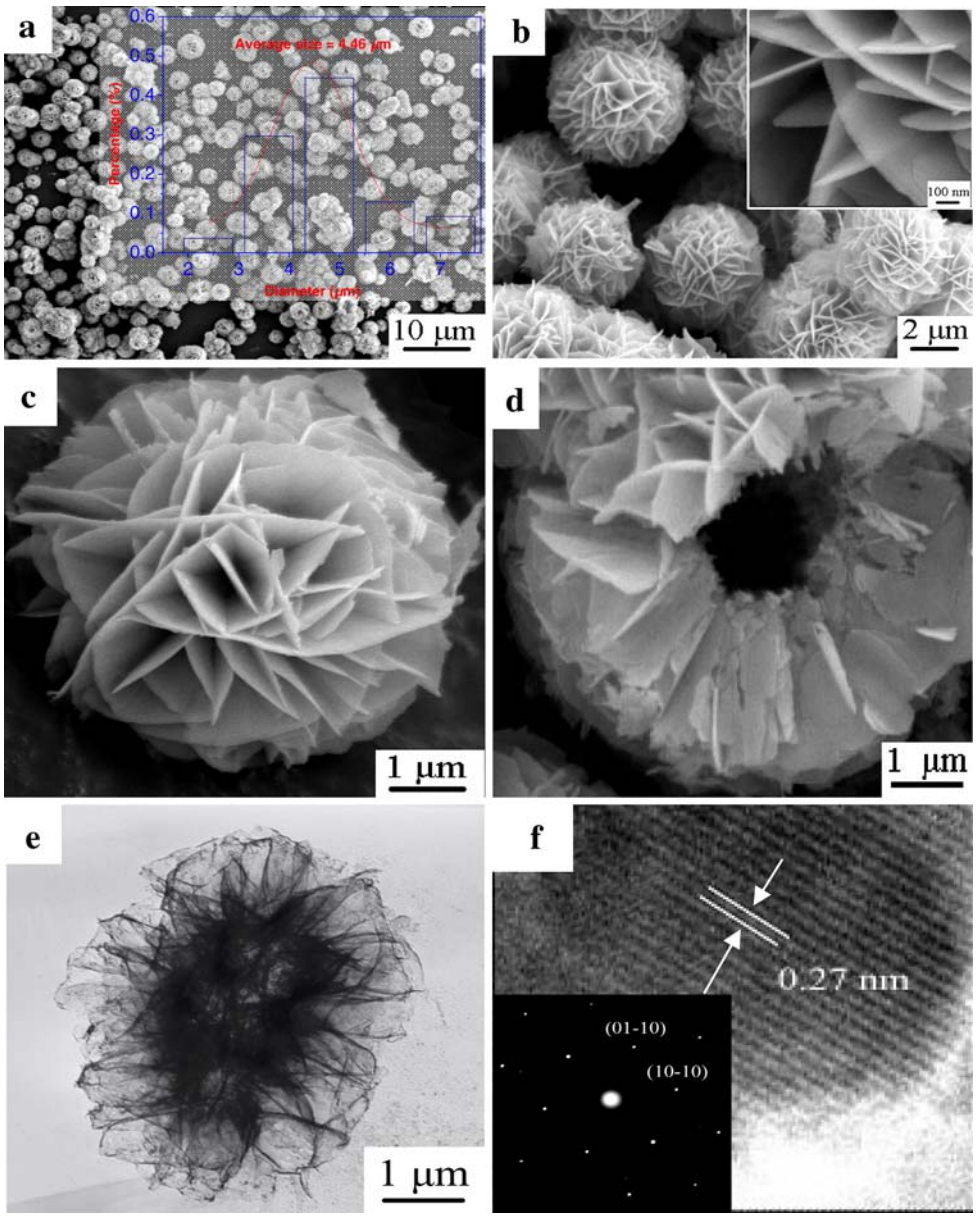

Fig. 2 **a–d** SEM images with different magnifications of the as-obtained β-Ni(OH)$_2$ samples. Inset of **a**: the size distribution of the as-synthesized sample; **e** TEM image of one typical hierarchical hollow architectures; **f** HRTEM image taken from the age of the hexagonal phase β-Ni(OH)$_2$ sheets and the corresponding selected-area electron diffraction (SAED) pattern (*lower left corner*)

To further obtain structural information for the well-aligned sheets, high-resolution TEM (HRTEM) images and the corresponding selected area electron diffraction (SAED) patterns were also recorded on single sheet. In a HRTEM image (Fig. 2f) taken from the edge of a sheet, the lattice fringes are clearly visible with a spacing of 0.27 nm, which is in good agreement with the spacing of the (01-10) planes of β-$Ni(OH)_2$ (JCPDS No: 14-0117). The corresponding SAED pattern is shown in the inset of Fig. 2f. The SAED and HRTEM analyses reveal that the building units are single-crystal.

In order to reveal the formation process of the 3D flower-like hollow architectures in more detail, time-dependent experiments were carried out and the resultant products were analyzed by TEM. The representative TEM images of the products prepared at certain reaction time intervals are shown in Fig. 3. Under the present synthetic conditions, nanoparticles and some ultra-thin nanosheets can be obtained as a result of aggregation and growth after treatment for 2 h (Fig. 3a). When the reaction time was prolonged to 6 h, besides flower-like hollow architectures, some underdeveloped flower-like hollow architectures also existed in the as-synthesized samples, as shown in Fig. 3b, indicating that oriented attachment is still underway. After the reaction was further prolonged to 12 h, fully developed 3D flower-like hierarchical hollow architectures similar to that shown in Fig. 2 are observed (Fig. 3c).

In addition, the roles of urea and ammonia were found to be very important for the formation feature of 3D flower-like hollow architectures. In a control experiment, when no urea was added under the same reaction conditions, the products take on a flake-like shape (Fig. 3d) rather than 3D

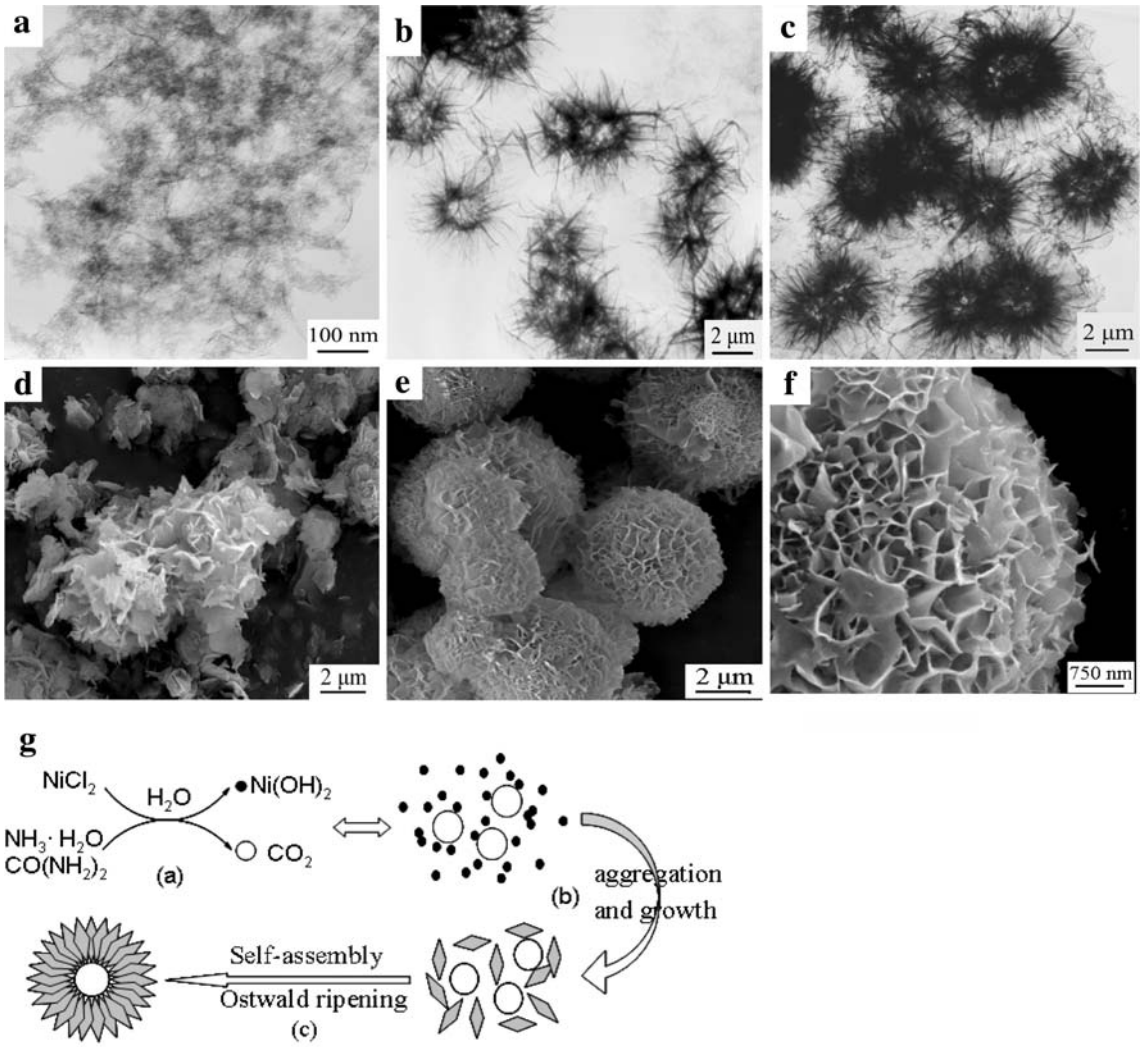

Fig. 3 TEM images of the as-synthesized samples with treatment times of **a** 2 h, **b** 6 h, and **c** 12 h at 120 °C. SEM images of the as-synthesized sample obtained at 120 °C for 12 h: **d** without urea; **e** and **f** without ammonia; **g** schematic illustration of the formation of β-$Ni(OH)_2$ 3D flower-like hollow architectures

flower-like hierarchical hollow architectures, while the ammonia was absent, only honeycomb-structured microarchitectures can be obtained, as shown in Fig. 3e and f.

On the basis of the above results in the present study, we believe that urea, ammonia, and reaction time play important roles in the formation of 3D flower-like hollow architectures. The formation of 3D flower-like hierarchical hollow architectures may result from the combined roles of urea, ammonia under the appropriate reaction condition. The chemical reaction in the process to obtain $Ni(OH)_2$ 3D flower-like hollow microarchitectures could be formulated as follows:

$$Ni^{2+} + 6NH_3 \leftrightarrow \left[Ni(NH_3)_6\right]^{2+} \quad (1)$$

$$CO(NH_2)_2 + H_2O \rightarrow 2NH_3 + CO_2 \uparrow \quad (2)$$

$$NH_3 + H_2O \rightarrow NH_4^+ + OH^- \quad (3)$$

$$Ni^{2+} + 2OH^- \rightarrow Ni(OH)_2 \downarrow \quad (4)$$

Most probably, the bubbles of CO_2 gas produced in the reaction with the participation of $CO(NH_2)_2$ must have played a key role, since no other templates/surfactants/emulsions were used in this work. A possible formation process involving the assembly-then-assemble mechanism can be schematically illustrated in Fig. 3g. In the beginning, Ni^{2+} in solution reacts first with NH_3 to form a relatively stable complex, $[Ni(NH_3)_6]^{2+}$, because of its strong affinity to Ni^{2+} at room temperature. Afterwards, the complex was decomposed and released NH_3 to provide OH^- ions for the formation of $Ni(OH)_2$ by a hydrothermal treatment. At the same time, with the participation of $CO(NH_2)_2$, many micrometer/sub-micrometer CO_2 bubbles are produced in the system at 120 °C (step a). The freshly crystalline nanoparticles are unstable because of their high surface energy and tend to aggregate and form higher nanoparticles, driven by the minimization of interfacial energy. In our synthesis, the formation of $[Ni(NH_3)_6]^{2+}$ complex would sharply decreased the free Ni^{2+} concentration in the solution, which resulted in a relatively low reaction rate of Ni^{2+} ions with OH^- ions. A slow reaction rate caused the separation of nucleation and growth steps, which is crucial for high-quality crystal synthesis. As a result, the sheet-like high crystalline $Ni(OH)_2$ was firstly formed (step b), which may be related to the nature of the initial crystal structures [34]. Then the self-assembly and Ostwald ripening process occurs around the gas/liquid interface of CO_2 and water, and finally 3D flower-like hierarchical hollow architectures (step c). Here, CO_2 bubbles decomposed from $CO(NH_2)_2$ can act as soft templates to induce the self-assembly of nanosheets on their surfaces. A similar gaseous bubble has also been used as a template for TiO_2 and VOOH hollow nanostructures [35, 36], which is different from the assembly-then-inside-out evacuation mechanism in the formation of Fe_3O_4 hollow spheres [37]. Our time-dependent experiments support the above aggregation-then-assembly mechanism; it is found that the assembly process occurs after the formation of the nanosheets.

The thermal behavior of flower-like hierarchical β-$Ni(OH)_2$ hollow architectures was investigated with TG and DSC measurements (Fig. 4). A TG curve showed that β-$Ni(OH)_2$ started to decompose (weight loss) at about 285 °C. The total weight loss was measured to be ~22% which is larger than the theoretical value (19.4%) calculated from the following reaction:

$$Ni(OH)_2 \rightarrow NiO + H_2O \quad (5)$$

The powders exhibit thermogravimetric transitions that are likely due to the loss of physical absorbed and structural water. The initial weight loss from 30 to 140 °C is attributed to the loss of surface adsorbed water and ethanol. The weight loss in the range of 140–365 °C is due to the removal of the crystalline water molecules. After 365 °C, the weight loss continued but gradually slowed at 400 °C and almost ceased at 500 °C. As a consequence, the stable residue can reasonably be ascribed to NiO. The DSC curve showed an endothermic peak with a maximum located at 315 °C. The temperature range of the endothermic peak in the DSC curve fits well with that of weight loss in the TG curve, corresponding to endothermic behavior during the decomposition of β-$Ni(OH)_2$ to NiO.

The nickel hydroxyl can easily be transformed to NiO upon heat treatment. Figure 5 shows the XRD patterns of the flower-like hierarchical β-$Ni(OH)_2$ hollow architectures heated at various temperatures. All the diffraction peaks can be indexed to the face-centered cubic (fcc) NiO phase (JCPDS No. 04-0835). No peaks due to β-$Ni(OH)_2$ are observed, suggesting that β-Ni $(OH)_2$ is completely

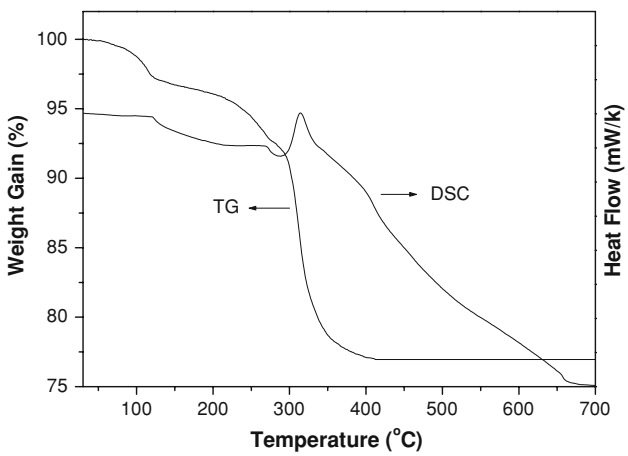

Fig. 4 Differential scanning calorimetric analysis (DSC) and thermogravimetric analysis (TG) curves of β-$Ni(OH)_2$ 3D flower-like hollow architectures

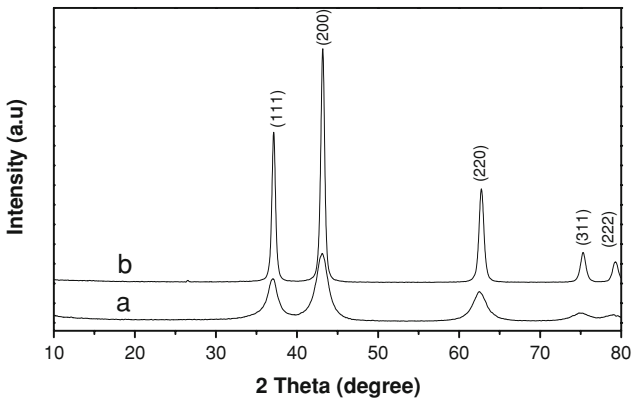

Fig. 5 XRD patterns of the as-obtained β-Ni(OH)$_2$ samples calcined at different temperatures for 4 h: (a) 300 °C and (b) 500 °C

converted to NiO after being heated for 4 h, which is also confirmed by TG and DSC studies. Notably, when increasing calcination temperature to 500 °C, all the peaks belonging to NiO cubic phase were markedly sharpening with high intensities, which suggested that the crystallinity of NiO phase was higher at high calcination temperature than that obtained at low calcination temperature.

The corresponding SEM images and EDS patterns are presented in Fig. 6. It can be observed from Fig. 6a, after annealing for 4 h in air, the morphology and structure of the flower-like hierarchical hollow architectures were sustained very well, which may due to the in situ conversion of β-Ni(OH)$_2$ nanosheets to NiO nanosheets [23]. In addition, the nanocontact between particles may also stabilize the 3D flower-like structure mechanically against collapse or fracture [27]. The magnified SEM image shown in Fig. 6b and c displays that pores were produced among the nanosheets. This kind of porous structure was formed due to the dehydration and decomposition of Ni(OH)$_2$ during heating. The EDS result shown in Fig. 6d demonstrates that the as-prepared sample contains Ni and O, and the atomic ratio of Ni and O is ~44.01:40.14, which agrees well with the stoichiometry of NiO. The Au peaks come from the thin gold layer for conductive coating (the signal of C is from the conductive adhesive). Shown in the inset of Fig. 6d is the SAED pattern that was recorded from the individual nanosheet, which can be indexed to the face-centered cubic structure with phase purity. It is interesting and surprising that the porous nanosheet still exhibits an almost single-crystalline diffraction pattern. Here, heat treatment may provide the energy to make the NiO particles self-assembled with high orientation and kept the former single-crystalline nature of the sheets [38].

The UV–Vis absorption spectrum of the sample is presented in Fig. 7. The strong absorption in the UV region can be observed, which is attributed to the band gap absorption of the as-synthesized NiO sample. In principle, the optical band gap energy E_g for a semiconductor can be estimated by the equation [39]:

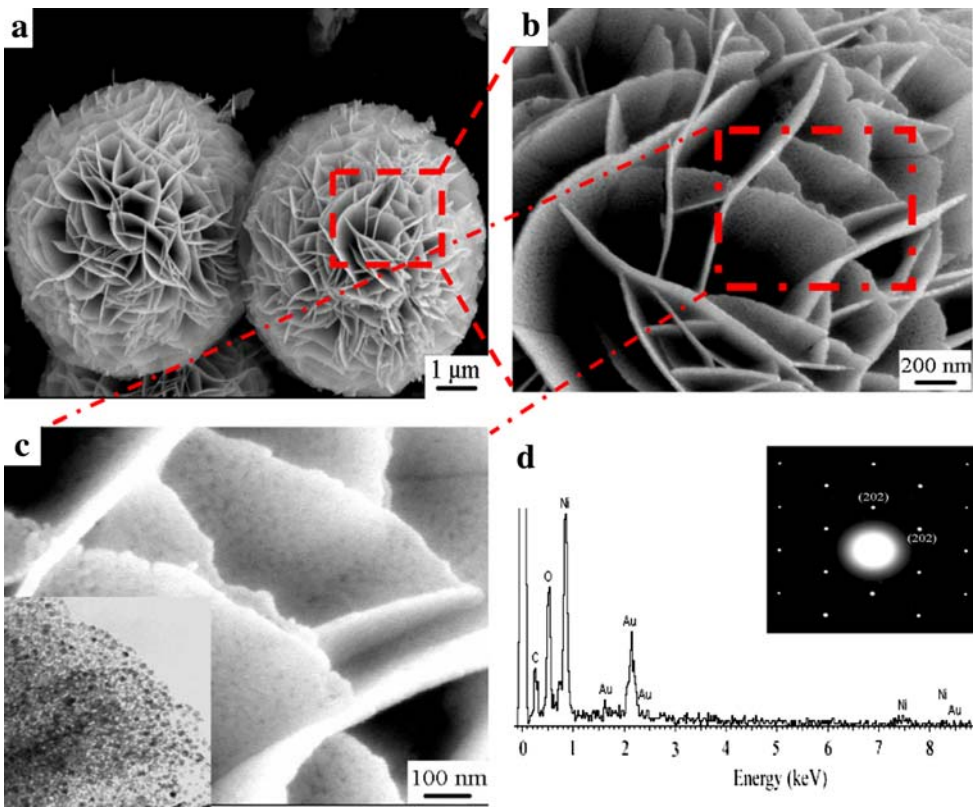

Fig. 6 **a** SEM image of double typical 3D flower-like hierarchical NiO architectures; **b–c** the corresponding enlarged SEM images of the area marked with a red rectangle. Inset **c** is a high-magnification TEM image of a sheet; **d** EDS result of the as-obtained β-Ni(OH)$_2$ samples calcined at 500 °C for 4 h. Inset of **d** shows SAED pattern of the NiO nanosheet

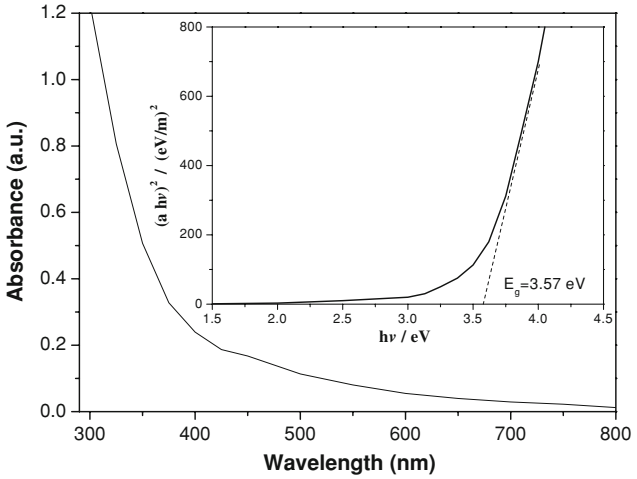

Fig. 7 UV–Vis absorption spectrum for the as-synthesized NiO samples. The inset is the $(\alpha hv)^2$–hv curve

$$(\alpha hv)^n = B\left(hv - E_g\right) \tag{6}$$

where α is the absorption coefficient, hv is the photon energy, B is a constant relative to the materials n is either 2 for direct inter-band transition or 1/2 for indirect inter-band transition [27]. The inset of Fig. 7 shows the $(\alpha hv)^2$–hv curve for the sample. The band gap of the as-synthesized NiO samples was about 3.57 eV by the extrapolation of the above equation, which shows obvious red-shift compared with that of the bulk NiO (4.0 eV) [40]. Such a difference could be contributed to their spherical hollow hierarchical architectures and the small thickness of the sheets with porous structures, in which the interactions between the connected building blocks led to a quantum size effect [41]. No linear relation was found for $n = 1/2$, indicating that the as-prepared NiO samples have a direct band gap.

Conclusions

The 3D flower-like hierarchical β-Ni(OH)$_2$ hollow architectures have been synthesized by a facile hydrothermal route in the presence of urea and ammonia. The 3D flower-like hollow architectures with the size of several micrometers are composed of nanosheets of 10–20 nm in thickness. The results indicated that the reaction time, urea and ammonia play important roles in the formation of 3D flower-like hierarchical β-Ni(OH)$_2$ hollow architectures. By calcining the as-prepared flower-like β-Ni(OH)$_2$ hollow architectures, hierarchical NiO crystallites with porous single-crystalline nanosheets were obtained, well inheriting the shapes of the β-Ni(OH)$_2$ samples. The optical absorption band gap of the as-obtained NiO samples is determined to be 3.57 eV. Due to the unique architectures, the as-obtained products may have potential applications in water treatment, electrode, sensors, catalysts, biomarkers, microelectronics, energy storage, and other related micro/nanoscale devices due to their unique architectures.

Acknowledgments This work was financially supported by the National Natural Science Foundation of China (Nos.: 50573090 and 10672161) and Beijing Municipal Natural Science Foundation (No. 2082023).

References

1. G. Kaltenpoth, M. Himmelhaus, L. Slansky, F. Caruso, M. Grunze, Adv. Mater. **15**, 1113 (2003). doi:10.1002/adma.200304834
2. Y. Hou, H. Kondoh, T. Ohta, Chem. Mater. **17**, 3994 (2005). doi:10.1021/cm050409t
3. L.P. Zhu, H.M. Xiao, W.D. Zhang, Y. Yang, S.Y. Fu, Cryst. Growth Des. **8**, 1113 (2008). doi:10.1021/cg701036k
4. L.P. Zhu, W.D. Zhang, H.M. Xiao, Y. Yang, S.Y. Fu, J. Phys. Chem. C **112**, 10073 (2008). doi:10.1021/jp8019182
5. J. Yuan, K. Laubernds, Q. Zhang, S.L. Suib, J. Am. Chem. Soc. **125**, 4966 (2003). doi:10.1021/ja0294459
6. M. Yada, C. Taniguchi, T. Torikai, T. Watari, S. Furuta, H. Katsuki, Adv. Mater. **16**, 1448 (2004). doi:10.1002/adma.200306676
7. J. Hu, L. Ren, Y. Guo, H. Liang, A. Cao, L. Wan, C. Bai, Angew. Chem. Int. Ed. **44**, 1269 (2005). doi:10.1002/anie.200462057
8. L.P. Zhu, H.M. Xiao, X.M. Liu, S.Y. Fu, J. Mater. Chem. **16**, 1794 (2006). doi:10.1039/b604378j
9. S.A. Jenekhe, X.L. Chen, Science **279**, 1903 (1998). doi:10.1126/science.279.5358.1903
10. J. Du, Y. Chen, Angew. Chem. Int. Ed. **43**, 5084 (2004). doi:10.1002/anie.200454244
11. X.W. Lou, C. Yuan, E. Rhoades, Q. Zhang, L.A. Archer, Adv. Funct. Mater. **16**, 1679 (2006). doi:10.1002/adfm.200500909
12. Y. Yin, R.M. Rioux, C.K. Erdonmez, S. Hughes, G.A. Somorjai, A.P. Alivisatos, Science **304**, 711 (2004). doi:10.1126/science.1096566
13. S. Park, J.H. Lim, S.W. Chung, C.A. Mirkin, Science **303**, 348 (2004). doi:10.1126/science.1093276
14. B. Liu, H.C. Zeng, J. Am. Chem. Soc. **126**, 8124 (2004). doi:10.1021/ja048195o
15. P.F. Noble, O.J. Cayre, R.G. Alargova, O.D. Velev, V.N. Paunov, J. Am. Chem. Soc. **126**, 8092 (2004). doi:10.1021/ja047808u
16. H.M. French, M.J. Henerson, A.R. Hillman, E. Vieil, J. Electroanal. Chem. **500**, 192 (2001). doi:10.1016/S0022-0728(00)00373-9
17. X.H. Liu, L. Yu, J. Power Sources **128**, 326 (2004). doi:10.1016/j.jpowsour.2003.10.006
18. X.J. Han, X.M. Xie, C.Q. Xu, D.R. Zhou, Y.L. Ma, Opt. Mater. **23**, 465 (2003). doi:10.1016/S0925-3467(02)00340-3
19. J.H. Liang, Y.D. Li, Chem. Lett. **32**, 1126 (2003). doi:10.1246/cl.2003.1126
20. D.N. Yang, R.M. Wang, J. Zhang, Z.F. Liu, J. Phys. Chem. B **108**, 7531 (2004). doi:10.1021/jp0375867
21. F. Tao, M. Guan, Y. Zhou, L. Zhang, Z. Xu, J. Chen, Cryst. Growth Des. **8**, 2157 (2008). doi:10.1021/cg7012123
22. X. Ni, Q. Zhao, B. Li, J. Cheng, H. Zheng, Solid State Commun. **137**, 585 (2006). doi:10.1016/j.ssc.2006.01.033
23. D. Wang, C. Song, Z. Hu, X. Fu, J. Phys. Chem. B **109**, 1125 (2005). doi:10.1021/jp046797o
24. Y. Wang, Q. Zhu, H. Zhang, Chem. Commun. 5231 (2005). doi:10.1039/b508807k

25. G. Duan, W. Cai, Y. Luo, F. Sun, Adv. Funct. Mater. **17**, 644 (2007). doi:10.1002/adfm.200600568
26. L. Yang, Y. Zhu, H. Tong, Z. Liang, W. Wang, Cryst. Growth Des. **7**, 2716 (2007). doi:10.1021/cg060530s
27. Y. Luo, G. Duan, G. Li, J. Solid State Chem. **180**, 2149 (2007). doi:10.1016/j.jssc.2007.05.025
28. L. Xu, Y.-S. Ding, C.-H. Chen, L. Zhao, C. Rimkus, R. Joesten, S.L. Suib, Chem. Mater. **20**, 308 (2008). doi:10.1021/cm702207w
29. J. He, M. Lindstrom, A. Hagfeldt, S.E. Lindquist, J. Phys. Chem. B **103**, 8940 (1999). doi:10.1021/jp991681r
30. H.P. Stadniychuk, M.A. Anderson, T.W. Chapman, J. Electrochem. Soc. **143**, 1629 (1996). doi:A1996-14-8115L-006
31. M. Yoshio, Y. Todorov, K. Yamato, H. Noguchi, J. Itoh, M. Okada, T. Mouri, J. Power Sources **74**, 46 (1998). doi:10.1016/S0378-7753(98)00011-1
32. D. Wang, R. Xu, X. Wang, Y. Li, Nanotechnology **17**, 979 (2006). doi:10.1088/0957-4484/17/4/023
33. L. Xiang, X.Y. Deng, Y. Jin, Scr. Mater. **47**, 219 (2002). doi:10.1016/S1359-6462(02)00108-2
34. P. Benito, F.M. Labajos, V. Rives, J. Solid State Chem. **179**, 3784 (2006). doi:10.1016/j.jssc.2006.08.010
35. X. Li, Y. Xiong, Z. Li, Y. Xie, Inorg. Chem. **45**, 3493 (2006). doi:10.1021/ic0602502
36. C. Wu, Y. Xie, L. Lei, S. Hu, C. OuYang, Adv. Mater. **18**, 1727 (2006). doi:10.1002/adma.200600065
37. L.P. Zhu, H.M. Xiao, W.D. Zhang, G. Yang, S.Y. Fu, Cryst. Growth Des. **8**, 957 (2008). doi:10.1021/cg700861a
38. Z. Gui, J. Liu, Z. Wang, L. Song, Y. Hu, W. Fan, D. Chen, J. Phys. Chem. B **109**, 1113 (2005). doi:10.1021/jp047088d
39. J. Pankove, *Optical Processes in Semiconductors* (Prentice-Hall, Englewood Cliffs, NJ, 1971)
40. A.J. Varkey, A.F. Fort, Thin Solid Films **235**, 47 (1993). doi:10.1016/0040-6090(93)90241-G
41. Y. Lin, T. Xie, B. Cheng, B. Geng, L. Zhang, Chem. Phys. Lett. **380**, 521 (2003). doi:10.1016/j.cplett.2003.09.066